Application of spatial transcriptomics across organoids: a high-resolution spatial whole-transcriptome benchmarking dataset

Nucera MR[1,2,3*], Charitakis N[1,2,3*], Leung RF[1,2,3*], Leichter A[1,2], Tuano N[1,2], Walkiewicz M[1,2], Sawant V[1,2,3], Rowley L[1,2], Scurr M[1,2], Er PX[1,2], Tan KS[1,2], Sutton R[1,2], Ahmad F[1,2], Saxena R[1,2,3], Maytum A[1,2], Turner D[1,2,3], Voges HK[1,2,3], Nim HT[1,2], Sun X[4], Yang B[4], Li KL[4], Ball G[3,5], Elefanty AG[1,2,3], Lamandé SR[1,2,3], Lawlor KT[1,2,3], Vanslambrouck JM[1,2,3], Mills RJ[1,2,,3,6], Ng ES[1,2,3], Stanley EG[1,2,3], Werder RB[1,2,3], Little MH[1,2,3,7], Elliott DA[,2,3,8,,9], Porrello ER[1,2,3,9,10], Faux MC[1,3,11#], Eisenstat DD[1,3,12#], Velasco S[1,2,3,#], Rossello FJ[1,2,3,13,#,+], Ramialison M[1,2,3,14,#,+]

[1] Stem Cell Medicine Theme, Murdoch Children's Research Institute, Parkville, VIC, Australia.
[2] The Novo Nordisk Foundation Center for Stem Cell Medicine, reNEW Melbourne, Murdoch Children's Research Institute, Parkville, VIC, Australia.
[3] Department of Paediatrics; University of Melbourne; Parkville, VIC, Australia.
[4] BGI Australia, Brisbane, QLD, Australia.
[5] Developmental Imaging, Murdoch Children's Research Institute, Parkville, VIC, Australia.
[6] School of Biomedical Sciences, Queensland University of Technology, Brisbane, QLD, Australia
[7] The Novo Nordisk Foundation Center for Stem Cell Medicine, reNEW Copenhagen, University of Copenhagen, Denmark.
[8] Australian Regenerative Medicine Institute, Monash University, Melbourne, VIC, Australia.
[9] Melbourne Centre for Cardiovascular Genomics and Regenerative Medicine, Melbourne, VIC, Australia.
[10] Department of Anatomy and Physiology, School of Biomedical Sciences, The University of Melbourne, Melbourne, VIC, Australia.
[11] Department of Surgery, The University of Melbourne, Parkville, VIC, Australia.
[12] The Royal Children's Hospital, Parkville, VIC, Australia.
[13] Department of Clinical Pathology, University of Melbourne, Melbourne, VIC, Australia.
[14] Systems Biology Institute, Clayton, VIC, Australia.
[#]co-senior authors
[+]corresponding authors Fernando.rossello@mcri.edu.au; mirana.ramialison@mcri.edu.au

Summary

Stem cell-derived organoid models hold great promise to model tissue-specific disease. To enable this, it is crucial to determine how their composition compares to endogenous organs. However, technologies such as spatial transcriptomics (STs) that can inform on regional molecular identity have been challenging to apply to organoids. Here we present the first systematic profiling of multiple organoids (brain, heart muscle, heart valve, kidney, lung, cartilage, and blood) using Stereo-seq. We describe the optimisation of ST with multiple organoids on a single chip. We reveal differences in data capture efficiency compared to reference tissues hindering traditional downstream analyses. To overcome such challenges, we developed a bespoke regional analysis method to enable detection of transcriptional changes. Together, these developments form a platform to inform future work to investigate organoids using ST, both in terms of optimising data capture of multiple organoids across a chip and novel methods for regional analysis of organoids.

Introduction

Pluripotent stem cells (PSCs) derived organoid models are used to investigate human development and disease pathogenesis and provide a platform to measure drug response (D. Zhao et al., 2021). This requires organoids to accurately recapitulate *in vivo* embryonic and adult organs, both physiologically and in cellular composition, by replicating the process of stem cell development and organization (Prasad et al., 2021; Z. Zhao et al., 2022). Pluripotent stem cells (PSCs) derived organoid models can be used to investigate human development and disease pathogenesis and provide a platform to measure drug response (D. Zhao et al., 2021). This requires models of human tissues that accurately recapitulate their *in vivo* counterparts, both physiologically and in cellular composition. The heterogeneous nature and spatial organisation of cell populations within organoids warrants the use of spatial transcriptomics to investigate tissue formation and disease pathogenesis (D. Zhao et al., 2021).

Spatial transcriptomics (ST) capture gene expression across tissues while maintaining spatial information. ST encompasses a wide array of technologies that are divided into imaging- and sequencing-based assays (Waylen et al., 2020). This study focuses on the application of Stereo-seq, a sequencing-based technology capable of capturing transcriptome-wide gene expression at single cell resolution (Chen et al., 2022). Stereo-seq profiles an embedded tissue section using a specialised chip, that simultaneously allows mRNA capture and imaging. Given the high cost of ST experiments and the relatively small size of organoids, finding a cost-effective approach to profile multiple organoids using a single chip is critical. While ST has previously been applied to single organoid models (Chiaradia et al., 2023; Ma et al., 2024; Wahle et al., 2023), technical challenges arise due to their small size. Indeed, only a limited portion of the ST chips are covered by organoid tissue. This may result in artificially lower mRNA levels or capture of fewer gene transcripts, which we define throughout as the total data capture. However, studies that compare mRNA expression and gene profiling of organoids using the Stereo-seq platform to endogenous tissue, for which the platform was originally optimised, are lacking. Furthermore, the placement of multiple organoids on a single chip has proven to be viable for certain organoid types (Ma et al., 2024), yet studies describing the feasibility and benefits of simultaneously placement of multiple organoid conditions on the same chip is limited.

In this study, we perform a systematic spatial transcriptome profiling of multiple organoid models (brain, heart muscle, heart valve, kidney, lung, cartilage, and blood) using the Stereo-

seq platform compared to two *in vivo* reference mouse tissues. First, we described the effective placement of multiple organoids and organoids of the same tissue type but cultured under different conditions on the same chip. We then tested the platform's capability to clearly distinguish transcriptional gene signatures from different samples on the same Stereo-seq chip. We investigated the effect of size, shape and cell-type composition of different organoids on data capture, when compared to one another and compared to larger, *in vivo* reference E13.5 mouse head and 21 PCW mouse heart tissues. Finally, despite challenges in cell type annotation, we illustrate an effective, alternative analysis for uncovering region-specific differences across organoids, enabling the identification of biologically relevant spatial expression patterns across organoids.

Results

We systematically profiled the spatial transcriptome of eight human organoid models (brain, lung, blood, transwell kidney, suspension kidney, heart valve, cartilage, and heart muscle) using the Stereo-seq platform. To capture multiple conditions within models, we designed a modified Stereo-seq workflow, where multiple organoids were co-embedded and placed on a single Stereo-seq chip (see Methods) (Fig. 1A). Tissue detachment from the chip surface was observed in cartilage, heart muscle and kidney organoids. To alleviate this, the modified Stereo-seq workflow included coating the chip with poly-L-lysine. Tissue-specific cell permeabilization required careful optimisation to limit transcript diffusion and allow for accurate spatial gene expression profiling. This optimization was critical to allow processing of multiple organoids and growth conditions on the same chip. In most organoid systems, we were able to optimise and identify suitable permeabilization conditions and therefore limit transcript diffusion (Fig. 1A). However, certain models such as blood and suspension kidney organoids displayed higher levels of transcript diffusion, indicated by transcripts captured outside of tissue locations, despite optimised permeabilization conditions (Fig. 1A).

To benchmark the performance of Stereo-seq on previously untested human organoid models, we also profiled two reference tissues (E13.5 mouse head and 21 PCW mouse heart) using the standard Stereo-seq workflow (Fig. 1A). To account for the custom Stereo-seq workflow and compensate for differences in capture across organoids, we developed a custom bioinformatics workflow, including region specific analysis (Fig. 1B). In detail, this workflow filtered out organoid models of low quality enabling the effect of increased chip coverage on data capture to be investigated through a variety of metrics (Figs. S1A-S1B). When evaluating data capture

on the smallest unit of analysis, we used the CellBin (equivalent to each cell visualised across ssDNA image) generated during pre-processing via cell-segmentation methods on the accompanying immunofluorescence image (ssDNA, Fig. 1A). Although large variations persisted in total number of transcripts captured between organoids and *in vivo* tissue reference (Figs. S1A-S1B), the capture level for both the number of genes and counts on a CellBin levels are similar across organoid models and reference *in vivo* tissues (Figs. 1C-1D). Thus, this indicates the variation was introduced by differences in chip coverage area, rather than organoid type, emphasised by a correlation in total counts with the size of tissue when comparing organoids passing QC filtering with *in vivo* reference tissue (Fig. S1C). Certain organoid chips, such as blood, displayed much higher data capture due to placement of a greater number of organoids on a single chip and increased transcript diffusion (Figs. S1A-S1B).

Next, we focused on analysing organoids which had a more uniform size and shape resulting in clearer signal capture across the chip. We compared individual brain, transwell kidney and cartilage organoids placed on the same chip against *in vivo* E13.5 mouse head and 21 PCW mouse heart references (Figs. S1D-1H). We observed minimal variation in data capture between brain, transwell kidney and cartilage organoid models of similar size (Figs. S1E-S1H). Finally, we investigated the percentage of CellBins expressing housekeeping genes *GAPDH*/*Gapdh* and *ACTB*/*Actb* across reference mouse tissues and individual brain and cartilage organoids (Figs. S2A-S2B). Differences in the levels of expression of housekeeping genes were seen across reference tissues and organoids, consistent with fluctuations of expression in different cell type populations also seen in single-cell RNA-Seq experiments (Figs. S2A) (Lin et al., 2019). As expected, expression remained homogenous, with no clear spatial patterns emerging for the expression of these genes across the for organoids passing QC filtering (Figs. S2A-S2C).

In addition to CellBin, Stereo-seq offers the option to analyse data on a square bin level, by grouping adjacent transcript capture areas together. Therefore, we subsequently investigated the effects of altering bin size, which determines the resolution of a defined region, ultimately to identify potential regional expression patterns and differences between *in vivo* reference tissues and organoids. The square bin sizes can be determined by users, with bin size of 20 approximately corresponding to the size of a single cell with an area of 10 μm^2(StereopyBin.). Given the smaller size of the organoids compared to the mouse reference tissue and the data capture variability (Fig. 1), we investigated the effect of bin size on capture of mRNA levels,

genes, and biological signal (Fig. 2). We found that increasing bin size from 50 to 75 to 100 (25 μm^2, 37.5 μm^2 and 50 μm^2 respectively) across the *in vivo* reference tissues did not result in coverage of bins across the tissue changing significantly as larger bins were removed due to filtering parameters when compared to accompanying immunofluorescence image of corresponding whole tissues (Fig. 1A, Figs. 2A-2B). Thus, mRNA capture across most of the *in vivo* mouse reference tissue is maintained regardless of bin size, indicating more effective transcript capture across these tissues. However, the same effect was not observed in brain and cartilage organoids, with higher bin drop-out rates with increasing bin size, resulting in a smaller area of the organoid being profiled (Figs. 2C-2D). The relatively low number of unique molecular identifiers (UMIs) and gene capture across individual organoids also indicates the inability to analyse tissues of this size with single-cell resolution using this platform (Figs. 2C-2D).

When binning data, the number of bins represents the total chip coverage area and tissue size. Across both *in vivo* references and different organoid models, we did not see a proportional decrease in the number of bins as bin size increased from 50 to 75 (Figs. $2E_{i\text{-}ii}$). Presumably, as the bin size increases by 50%, we would expect to see a 50% decrease in the number of bins to capture a similar tissue area. In both *in vivo* references, increasing the bin size by 50% led to the number of bins decreasing by more than half, while a doubling of bin size leads to retaining only about one-third of the total number of bins (Fig. $2E_i$). This effect was more noticeable across organoids (Fig. $2E_{ii}$), which might indicate greater inter-chip variability between organoids or greater variability between organoid size across chips. Furthermore, the difference in tissue size between *in vivo* reference tissues and organoids was emphasised by the difference in scale of the maximum number of bins captured at bin size 50 across organoids compared to in *in vivo* references (Fig. 2E). This means that even after significant decrease in number of bins across reference tissue adequate data remains for further downstream analysis. It is evident that increasing the bin size used for the analysis across organoid and reference tissues leads to a greater distribution in the number of genes captured per bin (Fig. 2F). This, along with the increase in area covered by each bin, results in heterogenous cell types being more likely to be included in larger bins, complicating clustering and cell-type identification.

To further investigate the effects of placing multiple organoids on a single chip, we compared normalisation across the entire chip compared to normalisation performed independently on individual organoids after subsetting (Fig. S3). Overall, the spatial expression of key

housekeeping or mitochondrial genes (*GAPDH*, *ACTB*, *MALAT1*, *MT-CO2*) or independent organoid marker genes remained unaffected across both methods of normalisation (Fig. S3). Evidence that normalisation did not skew biological signals is reflected in the homogeneous expression of *COL2A1*, *COL9A3* and *SPARC* across cartilage organoids, as expected, since they are composed of a single cell type.

Despite increasing bin sizes and normalisation, data generated from organoid experiments did not allow cell type classification and standard clustering analyses primarily due to insufficient granularity of transcriptional signatures. This was contrasted with the clear and accurate ST profiles generated from *in vivo* samples (Fig. S2C). Therefore, we developed an alternative analysis method that considers organoid regions to compare gene expression profiles in the border and core regions of organoids (Fig. 3A). We selected brain, transwell kidney, and cartilage organoids for this analysis, based on their comparable shape and size of each organoid of the same type, which allowed for benchmarking of the regional analysis method (Fig. 3 and Fig. S4A-S4I).

This analysis method successfully excluded any low-quality regions that potentially arose from inconsistent tissue adherence to the chip and therefore abnormal number of UMIs (Fig. 3C, Fig. S4A-S4D). Using this strategy, we showed that brain and cartilage organoids exhibited fewer outliers than kidney organoids likely due to their uniform shape and fewer scattered cells at the edge of the organoids (Fig S4D-S4F). This analysis also enabled the identification of corresponding edge, border, and core regions within the same and across different organoid types (Figs. 3D, Figs. S4E-S4F). We then determined differentially expressed genes (DEGs) between core and border regions of each organoid. Given the homogenous population that was expected in the cartilage organoids (Lamandé et al., 2023), no DEGs were identified between these regions (Fig. S4J). In brain organoids, we identified DEGs specific to the border or core regions, with 13 differentially upregulated in core regions and 13 in border regions (Fig. 3E). Using Gene Set Enrichment Analysis (GSEA), we further characterised the biological processes enriched in core and border regions of the brain organoids (Figs. 3F-3G). We found that border regions of brain organoids were enriched for gene sets related to ATP synthesis and electron transport (Fig. 3F), whereas core regions of the brain organoids were enriched for gene sets related to glycolysis (Fig. 3G). This aligns with previous studies showing enrichment of glycolytic gene sets in cortical neural progenitors which are located at the core of the organoid (Uzquiano et al., 2022) while more energy-demanding neuronal populations are found at the

border of organoids at this developmental stage. This shows that by using a region-specific analytical method we could identify spatially and metabolically distinct cell populations in brain organoids. These also resembles previous ST results generated using Slide-seq, an alternative sequencing ST technique (Uzquiano et al., 2022)

We applied our regional analysis method to validate its usage on irregularly shaped heart muscle organoids. These organoids have a figure eight shape, with two pole regions on either side of the organoid and the centre region that are amenable to live measurements of contractile functions (Fig. 4A-4B) (Mills et al., 2017). In this study, heart organoids were cultured under different conditions, one using previously published standard serum-free method (control) (Voges et al., 2023, Pocock et al 2024) and one using a directed maturation method (DM) for enhanced maturation and contractile force (Figs. 4A-4B) (Pocock et al., 2024). By applying the aforementioned region-specific analysis, pole regions were further filtered out from downstream analysis due to low cell density and transcript capture (Figs. 4A-4B). This demonstrates the utility of such analysis as a secondary quality control method based on tissue distribution. To validate the ST data capture quality, we performed pseudo-bulk analyses comparing centre regions of the control and DM organoids, using three organoids with best data capture across each condition selected (Fig. 4B, Fig. S4K-S4L). Although this approach does not account for spatially variable gene expression, we found significant differences in the transcriptomic profiles between the compared conditions (Fig. 4C). This illustrates the validity of ST technology in capturing conditional differences for samples on the same capture chip. Differential expression analyses identified the upregulation of *MRPS12*, a mitochondrial riboprotein, in the DM organoids (Fig. 4D), suggesting a difference in mitochondrial activity in more mature organoids. To identify altered biological processes, GSEA was performed (Figs. 4E-4F). In control heart organoids gene sets implicated in ion channel activities were enriched (Fig. 4E), while gene sets linked to mitochondrial activities, ATP synthesis, and metabolism were upregulated in DM heart organoids (Fig. 4F). Enrichment of these genes reflect recent findings that reported alternative usage of ion channels and increase in sarcomere maturity in more mature DM organoids, indicated through the downregulation of ion channel genes and upregulation of metabolic genes, respectively (Pocock et al., 2024). The transcriptional differences captured through ST between serum-free control and DM heart organoids resemble previous characterisation of these models, demonstrating the validity of single cell whole transcriptome ST in capturing transcriptional differences of organoids grown under different conditions.

Discussion

Recent advances in ST technology have resulted in the development of various platforms to provide an unbiased assessment of spatial gene expression profiles at subcellular level (Williams et al., 2022). In this study, we assessed the performance of single cell spatial transcriptomics by sequencing across eight different human organoid models and two mouse *in vivo* tissue references, with the objective of validating this technology across multiple tissue types in comparison to reference tissues, in which spatial gene expression profiles showed anatomical specificity and at single cell resolution. We identified technical challenges in applying ST on different organoid models, which included non-uniform transcript capture across chips, limited compatibility with certain organoid models, as well as failure to achieve single cell gene expression resolution.

We also tested the validity of placing multiple samples on the same chip. Previously, ST technology required single tissue sections to be placed on each chip to yield optimal outcome (Chiaradia et al., 2023; Ma et al., 2024; Wahle et al., 2023). Our analysis revealed that placing up to 12 sections on the same chip, as in the case of heart organoids, still resulted in accurate transcript capture. This was not limited to organoids of the same condition on the same chip, as we were able to delineate between organoids grown under different conditions, such as the case of serum-free vs DYMK heart organoids. The ability to maximise coverage with multiple sections per chip greatly extends the potential use of ST technology for organoids, ensuring high data value per chip and reduce inter-chip variability.

Across the eight organoid models assessed, cartilage, brain, and transwell kidney organoids resulted in sample quality comparable to tissue references, which could be attributed to their size and relatively uniform, round shapes. The expression of housekeeping genes such as *GAPDH* and *ACTB* were uniform across these organoids, although this was observed in less than 50% of the identified CellBins, resembling expression patterns seen in *in vivo* reference tissues. Gene expression at single cell resolution could not be achieved from these organoids, and, interestingly, decreasing resolution, *i.e.* increasing square bin sizes, did not resolve these challenges. This shows that while ST was able to capture transcripts from organoid models, region-specific expression patterns could not be identified. Furthermore, organoids with smaller surface areas, such as suspension kidney and blood organoids, despite comparable transcript capture and total gene counts, they displayed high amounts of diffuse gene

expression captured outside of the organoid surfaces. This was likely to be due to additional challenges presented by these 'liquid-phase' organoids resulting in transcript diffusion. Another challenge in applying Stereo-seq to these organoids was their lack of adhesiveness. As a remedy, poly-L-lysine chip coating was used to maximise tissue adhesion (see Methods). The data generated from heart organoids demonstrated that this method was effective in improving organoid adhesion and should be considered for all organoids to improve data quality.

Given the smaller size of organoids compared to *in vivo* tissue, the structural compartments in these models could be relatively subtle and marked by fewer cells. Coupled with the challenge of achieving single-cell resolution, the ability of ST technique in capturing spatially resolved gene expression in organoids and hence identification of defined patterning was limited. The use of cryo-sections may also limit the assessment of these organoids, as structural compartments could be rare and difficult to capture on a single cell-thick layer. These challenges demonstrate the need to further optimise protocols to apply ST to organoid models. Improvements could include applying alternative chip coating methods to further increase tissue adhesion or organoid fixation to better preserve spatial gene expression profiles. Additionally, as we have validated the use of multiple sections on a single chip, applying ST to multiple organoid sections and performing 3D reconstruction may more faithfully represent the organisation of cells within each system.

As standard clustering and cell type classification approaches were suboptimal for ST data generated from organoids, we developed an alternative regional analysis method that allowed spatial gene expression profiling in organoids. Through applying this analysis strategy on brain and heart organoids, we demonstrated its power in identifying region-specific biological processes as well as its utility as secondary quality control filter. This region-specific analysis method could be applied to further understand specific gene expression patterns in organoid models, useful to elucidate general structural organisation that may be present in these systems. This knowledge could then be used to further develop organoid models to better reflect their *in vivo* counterparts, especially organoid patterning for the study of developmental tissue patterning. These could have significant implications in developmental biology, such as identifying processes of cell differentiation.

Limitations of Study

Although we examined Stereo-seq ST technology across a wide range of organoids, other ST technologies may present different outcomes when applied to these systems. For instance, other sequencing-based ST technology such as 10x Visium HD, also offer single-cell resolution spatial gene profiling, and given the different chemistry and transcript capture technology this could produce alternative results (Oliveira et al., 2024). Probe-based imaging ST technology alternatively as an orthogonal approach may also perform differently, with sub-cellular resolution and higher specificity. To validate findings reported in this study, traditionally spatial gene expression profiling methods such *in situ hybridisation* or immunofluorescence could be performed to identify the accuracy of spatial gene expression patterns. Additionally, expanding the range of *in vivo* tissues to correspond to the organoid systems included, such as including mouse kidney and lung tissues, would provide an additional point of reference to validate the use of Stereo-seq ST technology on various organ and organoid systems.

Methods

Animal maintenance and ethics approval

All animals were housed in the Murdoch Children's Research Institute (MCRI) Disease Model Unit and all animal works performed were conducted under the approval and in compliance of the MCRI Animal Ethics Committee agreements (SPPL20327). Timed pregnant mice were sacrificed by cervical dislocation following MCRI AEC approved protocols at embryonic day 13.5 where the presence of a vaginal plug after mating indicated (E0.5). E13.5 mouse heads and 21 postconceptional week (PCW) mouse hearts were fresh frozen in OCT (SAKURA Cat# 4583) and stored at -80^{0}C until further processing.

Maintenance of induced pluripotent stem cells (iPSC)

PB001.1 iPSCs (male) (Vlahos et al., 2019) were used for blood organoid differentiation, CRL1502.2 iPSCs (female) (Vanslambrouck et al., 2019) were used for transwell kidney organoid differentiation, MAFB^{mTagBFP}:GATA3^{mCherry} reporter iPSCs (Vanslambrouck et al., 2019) were used for suspension kidney organoid differentiation, PB10.5 iPSCs (male) (Vlahos et al., 2019) were used for heart organoid differentiation. Brain organoids were generated from PB001.1 (Vlahos et al 2019), PB001.1 harbouring a heterozygous 1bp insertion at chr5:177,135,105 (c.2insG) and PB001.1 harbouring a homozygous 4bp deletion at chr5:177,135,106 (c.3_6delGGAT). BU3 NGST CRISPRi iPSCs (male) (Werder et al., 2022) were used for lung organoid differentiation. MCRIi019-A iPSCs (female) (Yammine et al., 2023) were used for cartilage organoid differentiation. *Mycoplasma* contamination in all iPSCs

were monitored and excluded by regular testing. Karyotyping of all iPSCs were performed regularly and no significant genomic imbalances were identified.

All iPSCs were grown on human embryonic stem cell (hESC)-qualified Matrigel Matrix (Corning Cat# 354277), with varying medium conditions. iPSCs used for differentiation of cartilage, transwell kidney, suspension kidney, and blood organoids were maintained in Essential 8 Medium (Thermo fisher Scientific Cat# A1517001). iPSCs used for lung organoid differentiations were maintained in StemFlex Medium (Thermo Fisher Scientific Cat# A3349401), whereas iPSCs for brain and heart organoid differentiation were maintained in mTESR Medium (Stem Cell Technologies Cat# 85857).

Organoid preparation for Stereo-seq

Eight organoid models were generated in accordance to previously described differentiation protocols, including airway and alveolar type 2 organoids (Abo et al., 2022; Hawkins et al., 2021; Jacob et al., 2017) blood organoids (Ng et al., 2024), heart organoids serum-free controls (Mills et al., 2017, Voges et al 2023, Pocock et al 2024), heart organoids with directed maturation (DM) (Pocock et al., 2024), cartilage organoids (Lamandé et al., 2023), heart valve organoids (Voges H. et al, 2025), transwell kidney organoids (Lawlor et al., 2021), suspension kidney organoids (Kumar et al 2019), and brain organoids (Paulsen et al., 2022). Specifically, following alterations were included in respective organoids to generate different experimental conditions. Both iPSC-derived lung organoids at air-liquid interface were infected on the apical surface with respiratory syncytial virus (RSV-A2, MOI 1) as previously described for SARS-CoV-2 (Huang et al., 2020). After 4 hours, the inoculum was removed and cells washed. Uninfected and infected samples were collected 72 hours post infection. From day 48, cartilage organoids were either grown without additional treatment for 14 days or treated as follows. Condition 1: cartilage organoids were cultured without additional treatment after day 48 for 7 days followed by addition of 10nM Triiodothyronine (Sigma Aldrich Cat# T6397) for 7 days, condition 2: cartilage organoids were cultured without additional treatment after day 48 for 7 days, followed by 7 days in osteogenic medium (Lamandé et al., 2023) and condition 3: cartilage organoids were grown with addition of 10nM Triiodothyronine for 7 days followed by 7 days in osteogenic medium. All cartilage organoid conditions were harvested at day 62. Brain organoids grown from all three cell lines were collected on day 31.

At the time of harvest, organoids were separated from culturing media and washed in PBS, then placed in pre-chilled OCT. Organoids were then transferred to plastic mould containing OCT, and frozen in an ethanol or isopropanol slurry. For brain organoids, three organoids were embedded together and placed on the chip, whereas four transwell kidney, and cartilage organoids were embedded together and placed on the same chip. Eighteen heart valve organoids were embedded together and placed on the same chip. Six heart organoids of each condition (serum-free and DM) were embedded together in an array of 12 organoids. Over 20 blood and suspension kidney organoids were embedded in a single mould. For lung organoids, a pair of airway and alveolar type 2 sections, either infected or non-infected, were embedded in OCT together. However, the uninfected airway section was lost during sample processing, resulting in only infected airway section present and alveolar type 2 sections remained.

Stereo-seq T-chip coating

For the heart muscle, heart valve, and cartilage organoids, the sections were mounted on poly-L-lysine coated Stereo-seq T-chip to enhance adhesion. Stereo-seq T-chips were washed using nuclease-free H_2O twice and dried, then coated with 100µL of 0.01% (w/v) poly-L-lysine (Sigma Aldrich Cat# P8920) for 10 minutes at room temperature. Post incubation, the chips were washed with nuclease-free H_2O twice, and dried on a 37ºC slide dryer.

Stereo-seq sample processing and library preparation

Samples were prepared and processed using the STOmics Transcriptomics kit (STOmics Cat# 111KT114) in accordance with manufacturer's instructions (BGI Stereo-seq Transcriptomics set for Chip-on-a-slide user manual version B) with slight variations. 10µm sections of mouse tissue samples including E13.5 heads and 21PCW hearts, brain organoids, kidney organoids, lung organoids, and blood organoids were cryo-sectioned on CM3050S cryostat (Leica) and mounted on room temperature T-chips, then processed according to the STOmics user manual. 10µm cryo-sections of cartilage, and blood organoids were placed on room temperature poly-L-lysine coated Stereo-seq T-chips, then processed according to the STOmics user manual. All cryo-sections were fixed in ice cold methanol for 30 minutes at -30ºC. Tissue section permeabilization times were as follows: lung, blood, transwell kidney, suspension kidney, and cartilage organoid sections were permeabilised for 12 minutes, mouse head and brain organoids for 15 minutes, heart organoids and engineered heart valves for 18 minutes, and mouse heart for 24 minutes. The cDNA purification and library preparation of each sample was constructed

using the STOmics library preparation kit (STOmics Cat# 111KL114) in accordance with manufacturer's instructions (BGI STOmics Stereo-seq Transcriptomics set for Chip-on-a-slide user manual version B). Quality of the final cDNA library size was assessed using D1000 Tapestation Reagent (Agilent Technologies Cat# 5067-5602) and Screentape (Agilent Technologies Cat# 5067-5582) and the concentration measured with Qubit dsDNA HS kit (Thermo Fisher Scientific Cat# Q33231). The sequencing of the libraries was performed at the BGI Oceanic headquarters using MGI DNBSEQ T7 sequencer, with 1260 million reads targeted recovery per sample.

Bioinformatics Workflow

Preprocessing

The stitched .czi files taken with the Z2 Axio Imager were processed through ImageStudio v 2.1.1 using the ssDNA setting for staining to ensure they passed QC. They were then transformed into tif files to ensure compatibility with the SAW pipeline. The paired FASTQ, mask and processed imaging files were then processed using the SAW pipeline v 6.12 using default parameters including cell binning. Files generated from mouse hearts were aligned to the reference genome GRCm39 while files generated from organoids were aligned to the reference genome GRCh38.

Analysis of organoids and reference tissues

All organoids and *in vivo* reference tissues was conducted using the Squidpy package v1.2.2 (Palla et al., 2022)and Stereopy package v1.2 (Fang et al., 2023) with Python v3.8.2.

Organoid-specific regional analysis to uncover spatially-restricted transcriptomic differences

Artifacts and outliers at the edge of the organoids were first filtered to retain biologically relevant spatial information, as these often contained abnormal amount of UMIs counts (Figs. 3A-3C, Figs. S4A-S4C). A systematic approach was employed, where bins located far from the organoid centres ('distant points') were first identified through a k-nearest neighbours (k-NN) approach. Distance points were defined as bins with abnormally high distances from its nearest neighbours (*i.e.* outliers) were filtered (Fig. 3C, Figs. S4D-S4F). As most of the distant points were spatially distant from organoid centres, and to prevent central hollow regions from being misclassified as outliers, we restricted this analysis to the edge of the organoids and excluded bins in organoid centres that had high distance. We then computed the convex hull

of using the remaining points to define the spatial boundary and subsequently spatial regions in each organoid. Based on the distance distribution, we defined three spatial cluster regions per organoid: edge points included bins within the 10th percentile of boundary distances, border points included bins with distances between the edge threshold and half of the maximum distance, and core points included bins with distances exceeding the border threshold (Fig. 3D, Figs. S4G-S4I).

For each of the brain, cartilage and transwell kidney organoids (which were all largely circular in shape), we first calculated the centroid of the spatial coordinates within the dataset using Squidpy v1.2.2 and Python version v3.8.2. The centroid coordinates were determined, and the Euclidean distance of each point from the centroid was computed. A threshold was applied to classify distant points. Specifically, we identified points with distances greater than the 90th percentile of all distances as "distant points." Then we proceeded to detect outliers, that are points located outside the organoid represented false signals. These artifacts needed to be systematically removed to ensure that only biologically relevant spatial information was retained. These artifacts were located at a distance from the rest of the organoid cells, making it necessary to apply a targeted filtering approach. To remove outliers, we applied a k-nearest neighbours (k-NN) approach using the NearestNeighbors function from sklearn v1.5.0 and ball_tree algorithm parameter. A k parameter of 10 was used for brain organoids and 250 for kidney and cartilage. Since most of the false signals were spatially distant from the organoid cells, k-NN was used to identify points with abnormally high distances to their nearest neighbours. However, to prevent central hollow regions from being misclassified as outliers, we restricted this analysis to the distant bins. For each distant bin, the average distance to its nearest neighbours was computed and standardized using a Z-score transformation. Bins with a Z-score greater than 2 were classified as outliers and subsequently removed from further analysis.

Following the removal of outliers, we computed the convex hull of the remaining bins to define the spatial boundary of the dataset. To further classify points into distinct spatial regions of the ‘edge’, ‘border’ and ‘core’, we calculated the minimum distance of each point to the convex hull boundary. Based on the distance distribution we classified each bin as either belonging to the: ‘edge’ for bins within the 10th percentile of boundary distances, ‘border’ for bins with distances between the edge threshold and half of the maximum distance, and ‘core’ for bins

with distances exceeding the border threshold. The 'edge' of the organoid often contained an abnormal number of counts and was removed from further analysis.

After spatial classification, we generated pseudo-bulk samples using core and border regions of individual organoids placed on the same chip and performed differential expression analysis between the core and border regions of the same organoid types. Pseudobulk was performed using the pydeseq2 v1.6.0 and decoupler v0.4.11 packages. The get_pseudobulk function was used to generate pseudobulk samples from the anndata object using the core and border regions from each kind of organoid. This was then built into a DeSeq2 object and differential expression analysis performed. We treated the organoids on the same chip as pseudo-replicates, as even if the organoids were not exactly biological replicates but belonged to either different lines subjected to editing (brain organoids) or different growing conditions (cartilage organoids), the aim of the analysis was to identify regional differences in general within the inner and outer areas of the organoids, regardless of the organoid conditions. Subsequently, we conducted Gene Set Enrichment Analysis (GSEA) to determine enriched pathways and biological processes associated with differentially expressed genes.

For the heart organoids which had an elliptic shape, to approximate the organoid boundary, a convex hull was computed using the set of spatial coordinates. Specifically, an algorithm (e.g., Quickhull) identified the smallest convex polygon capable of enclosing all points. Then each bin's distance to the convex hull boundary was computed by treating each bin's coordinates as a point and measuring its distance to the perimeter of the convex polygon. This metric provided an estimate of whether a bin was located near the tissue edge (small distance) or more centrally (larger distance). To remove perimeter effects and focus on interior tissue regions, bins in the lower 15th percentile of boundary distance were excluded. The remaining data (with distances above this threshold) formed the "filtered" subset of bins, considered representative of the tissue's interior.

The spatial coordinates of the filtered bins were then subjected to PCA. The first principal component (PC1) was assumed to capture the tissue's major "long axis." This vector (PC1) was used for subsequent segmentation of the tissue into poles and centre regions. Each filtered bin was projected onto the long-axis vector by calculating a dot product between the spot's spatial coordinates and the principal-axis vector. This yielded a one-dimensional scalar value for each spot, referred to as its "projected distance." The minimum and maximum projected distances defined the overall range (or "length") along this axis. The axis was then divided into

three segments of equal length, the first segment from the minimum projection to one-third of the total range, the middle segment covering the next one-third of the range and the final segment from two-thirds of the range to the maximum projection. Bins in the bottom or top third of this range were labelled as "pole," whereas spots in the central third were labelled as "centre." Differential expression analysis in pseudo-bulk was performed between centre of the serum free and directed maturation heart organoids.

Figure Legends

Figure 1 – Overview of quality metrics across multiple organoid types and *in vivo* reference tissues when captured using the Stereo-seq platform.
(A) Schematic of organoid models and *in vivo* reference tissues included on individual Stereo-seq chips. Areas of high count expression are visualised as UMI heatmaps while accompanying immunofluorescence images display regions of ssDNA capture across the chip.

(B) Schematic of, from sample preparation to data analysis. A total of 10 Stereo-seq chips, each containing a different tissue, were used. After initial quality assessment, eight chips were retained for downstream analysis. Four organoid models were selected for region-specific analysis patterns of gene expression.

(C) UMI counts per CellBin across each chip.

(D) Number of genes per Cellbin across each chip.

Figure 2 – Effect of increasing bin size (50, 75, 100) on spatial patterning and data visualisation across reference tissues and organoids.
(A) Immunofluorescence image of ssDNA capture and heatmaps visualising regions of high counts and genes per bin across reference tissue E13.5 mouse head at increasing bin sizes .

(B) Immunofluorescence image of ssDNA capture and heatmaps visualising counts and genes per bin across reference tissue 21 PCW mouse heart tissue at increasing bin sizes.

(C) Immunofluorescence image of ssDNA capture and heatmaps visualising counts and genes per bin across a single brain organoid at increasing bin sizes. Brain organoid 1 displayed in the heatmaps is highlighted in immunofluorescence image.

(D) Immunofluorescence image of ssDNA capture and heatmaps visualising counts and genes per bin across a single pseudo-replicate of cartilage organoid. Cartilage organoid 1 displayed in the heatmaps is highlighted in immunofluorescence image.

(E) Bar plots of total number of bins captured across tissue at different bin sizes. (i) Reference E13.5 mouse head and 21 PCW mouse heart tissue. (ii) Brain organoid 1 and Cartilage organoid 1.

(F) Distribution of number of genes captured in each bin at bin sizes 50, 75 and, 100 for reference E13.5 mouse head, 21 PCW mouse heart, brain organoid 1 and cartilage organoid 1.

Figure 3 – Analysis of spatially-restricted, differentially expressed genes across centre and border regions of brain organoid.
(A) Representative workflow of region-specific analysis between core and border regions of organoids.

(B) Heatmap of regions of high counts across brain organoid 1 using CellBin.

(C) Outlier CellBins identified and visualised in magenta across brain organoid 1, representing a false positive signal to be removed before region analysis.

(D) Edge, border and centre regions highlighted for analysis in brain organoid 1.

(E) Volcano plots of genes upregulated in core (visualised in red) and those upregulated in border region (visualised in blue) for brain organoid pseudo-replicates 1-4.

(F) Gene set enrichment analysis using genes upregulated in core of brain organoids.

(G) Gene set enrichment analysis using genes downregulated in core of brain organoids.

Figure 4 – Analysis of differentially expressed genes across centre regions of cardiac organoids of different conditions.
(A) Example of outlined centre (blue) and pole (orange) regions across DM and Control heart organoids.

(B) Overview of immunofluorescent organoids across Stereo-seq chip outlining placement of six DM organoids on the top and six control organoids on the bottom side of the chip.

(C) PCA plot of data from 3 centre regions of control organoids and 3 regions of DM organoids.

(D) Volcano plots of genes upregulated in centre of DM organoids (red) compared to genes upregulated in centre of control organoids (blue).

(E) Gene set enrichment analysis using genes upregulated in centre of control heart organoids.

(G) Gene set enrichment analysis using genes upregulated in centre of DM heart organoids.

Supplementary Figure 1- Overview of data capture across different organoids and *in vivo* reference tissues.
(A) Total DNA nanoballs captured across each Stereo-seq chip for different organoids and reference tissues.

(B) Total number of UMIs captured across each Stereo-seq chip for different organoids reference tissues.

(C) Correlation between total counts and number of CellBins across different organoids passing QC and reference tissues.

(D) Total number of CellBins across reference tissues and individual brain, kidney transwell and cartilage organoids.

(E) Distribution of number of counts per CellBin across reference tissues and single organoids from chips passing QC.

(F) Distribution of number of genes per CellBin across reference tissues and single organoids from chips passing QC.

(G) Distribution of number of counts per bin50 across reference tissues and single organoids from chips passing QC.

(H) Distribution of number of genes per bin50 across reference tissues and single organoids from chips passing QC.

Supplementary Figure 2 - Overview of data capture across different organoids and *in vivo* reference tissues.

(A) Bar plot of percentage of CellBins expression housekeeping genes GAPDH/Gapdh and ACTB/Actb across reference tissues and single organoids from chips passing QC.

(B) Heatmap of gene expression housekeeping and mitochondrial genes across brain, cartilage, heart muscle, kidney transwell and lung organoid chips compared *in vivo* reference tissue.

(C) Heatmap of tissue-specific marker gene expression across brain, cartilage, heart muscle, kidney transwell and lung organoid chips compared *in vivo* reference tissue.

Supplementary Figure 3 – Effect of application of normalisation across chip or per organoid on expression of housekeeping and marker genes for brain, cartilage and kidney transwell organoids.

Supplementary Figure 4 - Analysis of spatially-restricted, differentially expressed genes across centre and border regions for individual brain, cartilage and kidney transwell organoids.
(A) Heatmap of regions of high counts across brain organoid 2-3 using CellBin.

(B) Heatmap of regions of high counts across cartilage organoids 1-4.

(C) Heatmap of regions of high counts across kidney transwell organoid 1-2 using CellBin.

(D) Outlier CellBins identified and visualised in magenta across brain organoid 2-3, representing a false positive signal to be removed before region analysis.

(E) Outlier CellBins identified and visualised in magenta across cartilage organoid 1-4, representing a false positive signal to be removed before region analysis.

(F) Outlier cellbins identified and visualised in magenta across kidney organoid replicates 1-2, representing a false positive signal to be removed before region analysis.

(G) Edge, border and centre regions highlighted for analysis in brain organoid replicates 2-3.

(H) Edge, border and centre regions highlighted for analysis in cartilage organoids 1-4.

(I) Edge, border and centre regions highlighted for analysis in kidney organoids 1-2.

(J) Volcano plots of genes upregulated in core displayed in red and those upregulated in border region visualised in blue for cartilage organoid samples 1-4. The analysis did not return statistically significant differentially expressed genes.

(K) Heatmap of 3 selected control heart organoids and 3 selected DM organoids.

(I) Visualisation of centre and poles for 3 selected control heart organoids and 3 selected DM organoids.

Resource Availability

Lead Contact

Further information and requests for resources should be directed to and will be fulfilled by the lead contacts, Fernando Rossello (Fernando.rossello@mcri.edu.au) and Mirana Ramialison (mirana.ramialison@mcri.edu.au).

Data and code availability

- All original code is available on Github: https://github.com/Ramialison-Lab/StereoseqOrganoids

Acknowledgements

This work was supported by the Novo Nordisk Foundation Center for Stem Cell Medicine, reNEW, supported by Novo Nordisk Foundation grant number NNF21CC0073729; a BGI STOmics Grant to NC and MR. E.R.P. is supported by an Investigator Grant from the National Health and Medical Research Council of Australia (GNT2008376). H.K.V was supported by a Postdoctoral Fellowship (106645) from the National Heart Foundation of Australia. MR is funded by a Future Leader Fellowship (107328) from the Heart Foundation of Australia, a Human Frontiers Science Program Grant (RGP008/2024). MR and HTN are supported by an NHMRC Ideas Grant (APP1180905). Additional infrastructure funding to the Murdoch Children's Research Institute was provided by the Australian Government National Health and Medical Research Council Independent Research Institute Infrastructure Support Scheme. The Australian Regenerative Medicine Institute is supported by grants from the State Government of Victoria and the Australian Government.

Author contributions

Conceptualization: MN, NC, RFL, MR. Methodology: MN, NC, RFL, MR. Software: MN. Formal Analysis: MN. Investigation: MN, NC, RFL, AL, LR, RS, AM, MS, NT, VS, DT, MW, PXE, SKT, RS, FA, HV, HN. Resources: XS, BY, KLL. Data Curation: MN, NC, RFL. Writing Original Draft: MN, NC, RFL, FJR, MR. Writing review and editing: all authors. Supervision: SV, GB, MCF, DDE, FJR, MR, DAE, ERP, RJM. Funding acquisition: NC, MR, AGE, SRL, KTL, JMV, RJM, ESN, EGS, RBW, MHL, DAE, PER, HKV, MCF, DDE, SV.

Declarations of interest

H.K.V. is a co-inventor on a patent held by the Murdoch Children's Research Institute that relates to stem cell derivation of valve cells and tissues. E.R.P. and R.J.M. are co-inventors on patents relating to cardiac organoid maturation and cardiac therapeutics, and are co-founders, scientific advisors, and stockholders in Dynomics. F.J.R. receives institutional and salary support as a) a coinvestigator and subcontractor with the Peter MacCallum Cancer Centre for an investigator-initiated trial which receives funding support from Regeneron Pharmaceuticals; and b) a co-investigator on a translational research project funded by a Regeneron Pharmaceuticals grant.

Bibliography

Abo, K. M., Sainz De Aja, J., Lindstrom-Vautrin, J., Alysandratos, K.-D., Richards, A., Garcia-De-Alba, C., Huang, J., Hix, O. T., Werder, R. B., Bullitt, E., Hinds, A., Falconer, I., Villacorta-Martin, C., Jaenisch, R., Kim, C. F., Kotton, D. N., & Wilson, A. A. (2022). *R E S O U R C E A N D T E C H N I C A L A D V A N C E Air-liquid interface culture promotes maturation and allows environmental exposure of pluripotent stem cell-derived alveolar epithelium*. https://doi.org/10.1172/jci

Chen, A., Liao, S., Cheng, M., Ma, K., Wu, L., Lai, Y., Qiu, X., Yang, J., Xu, J., Hao, S., Wang, X., Lu, H., Chen, X., Liu, X., Huang, X., Li, Z., Hong, Y., Jiang, Y., Peng, J., … Wang, J. (2022). Spatiotemporal transcriptomic atlas of mouse organogenesis using DNA nanoball-patterned arrays. *Cell*, *185*(10), 1777-1792.e21. https://doi.org/10.1016/j.cell.2022.04.003

Chiaradia, I., Imaz-Rosshandler, I., Nilges, B. S., Boulanger, J., Pellegrini, L., Das, R., Kashikar, N. D., & Lancaster, M. A. (2023). Tissue morphology influences the temporal program of human brain organoid development. *Cell Stem Cell*, *30*(10), 1351-1367.e10. https://doi.org/10.1016/j.stem.2023.09.003

Fang, S., Xu, M., Cao, L., Liu, X., Bezulj, M., Tan, L., Yuan, Z., Li, Y., Xia, T., Guo, L., Kovacevic, V., Hui, J., Guo, L., Liu, C., Cheng, M., Lin, L., Wen, Z., Josic, B., Milicevic, N., … Xu, X. (2023). *Stereopy: modeling comparative and spatiotemporal cellular heterogeneity via multi-sample spatial transcriptomics*. https://doi.org/10.1101/2023.12.04.569485

Hawkins, F. J., Suzuki, S., Beermann, M. Lou, Barillà, C., Wang, R., Villacorta-Martin, C., Berical, A., Jean, J. C., Le Suer, J., Matte, T., Simone-Roach, C., Tang, Y., Schlaeger, T. M., Crane, A. M., Matthias, N., Huang, S. X. L., Randell, S. H., Wu, J., Spence, J. R., … Kotton, D. N. (2021). Derivation of Airway Basal Stem Cells from Human Pluripotent Stem Cells. *Cell Stem Cell*, *28*(1), 79-95.e8. https://doi.org/10.1016/j.stem.2020.09.017

Huang, J., Hume, A. J., Abo, K. M., Werder, R. B., Villacorta-Martin, C., Alysandratos, K. D., Beermann, M. Lou, Simone-Roach, C., Lindstrom-Vautrin, J., Olejnik, J., Suder, E. L., Bullitt, E., Hinds, A., Sharma, A., Bosmann, M., Wang, R., Hawkins, F., Burks, E. J., Saeed, M., … Kotton,

D. N. (2020). SARS-CoV-2 Infection of Pluripotent Stem Cell-Derived Human Lung Alveolar Type 2 Cells Elicits a Rapid Epithelial-Intrinsic Inflammatory Response. *Cell Stem Cell*, *27*(6), 962-973.e7. https://doi.org/10.1016/j.stem.2020.09.013

Jacob, A., Morley, M., Hawkins, F., McCauley, K. B., Jean, J. C., Heins, H., Na, C. L., Weaver, T. E., Vedaie, M., Hurley, K., Hinds, A., Russo, S. J., Kook, S., Zacharias, W., Ochs, M., Traber, K., Quinton, L. J., Crane, A., Davis, B. R., … Kotton, D. N. (2017). Differentiation of Human Pluripotent Stem Cells into Functional Lung Alveolar Epithelial Cells. *Cell Stem Cell*, *21*(4), 472-488.e10. https://doi.org/10.1016/j.stem.2017.08.014

Lamandé, S. R., Ng, E. S., Cameron, T. L., Kung, L. H. W., Sampurno, L., Rowley, L., Lilianty, J., Patria, Y. N., Stenta, T., Hanssen, E., Bell, K. M., Saxena, R., Stok, K. S., Stanley, E. G., Elefanty, A. G., & Bateman, J. F. (2023). Modeling human skeletal development using human pluripotent stem cells. *Proceedings of the National Academy of Sciences of the United States of America*, *120*(19). https://doi.org/10.1073/pnas.2211510120

Lawlor, K. T., Vanslambrouck, J. M., Higgins, J. W., Chambon, A., Bishard, K., Arndt, D., Er, P. X., Wilson, S. B., Howden, S. E., Sin Tan, K., Li, F., Hale, L. J., Shepherd, B., Pentoney, S., Presnell, S. C., Chen, A. E., & Little, M. H. (2021). Cellular extrusion bioprinting improves kidney organoid reproducibility and conformation. HHS Public Access. *Nat Mater*, *20*(2), 260–271. https://doi.org/10.6084/m9.figshare.12957122

Lin, Y., Ghazanfar, S., Strbenac, D., Wang, A., Patrick, E., Lin, D. M., Speed, T., Yang, J. Y. H., & Yang, P. (2019). Evaluating stably expressed genes in single cells. *GigaScience*, *8*(9). https://doi.org/10.1093/gigascience/giz106

Ma, S., Wang, W., Zhou, J., Liao, S., Hai, C., Hou, Y., Zhou, Z., Wang, Z., Su, Y., Zhu, Y., Dai, X., Zhao, Y., Liao, S., Cai, Y., & Xu, X. (2024). Lamination-based organoid spatially resolved transcriptomics technique for primary lung and liver organoid characterization. *Proceedings of the National Academy of Sciences of the United States of America*, *121*(46). https://doi.org/10.1073/pnas.2408939121

Mills, R. J., Humphrey, S. J., Fortuna, P. R. J., Lor, M., Foster, S. R., Quaife-Ryan, G. A., Johnston, R. L., Dumenil, T., Bishop, C., Rudraraju, R., Rawle, D. J., Le, T., Zhao, W., Lee, L., Mackenzie-Kludas, C., Mehdiabadi, N. R., Halliday, C., Gilham, D., Fu, L., … Hudson, J. E. (2021). BET inhibition blocks inflammation-induced cardiac dysfunction and SARS-CoV-2 infection. *Cell*, *184*(8), 2167-2182.e22. https://doi.org/10.1016/j.cell.2021.03.026

Mills, R. J., Parker, B. L., Quaife-Ryan, G. A., Voges, H. K., Needham, E. J., Bornot, A., Ding, M., Andersson, H., Polla, M., Elliott, D. A., Drowley, L., Clausen, M., Plowright, A. T., Barrett, I. P., Wang, Q. D., James, D. E., Porrello, E. R., & Hudson, J. E. (2019). Drug Screening in Human PSC-Cardiac Organoids Identifies Pro-proliferative Compounds Acting via the Mevalonate Pathway. *Cell Stem Cell*, *24*(6), 895-907.e6. https://doi.org/10.1016/j.stem.2019.03.009

Mills, R. J., Titmarsh, D. M., Koenig, X., Parker, B. L., Ryall, J. G., Quaife-Ryan, G. A., Voges, H. K., Hodson, M. P., Ferguson, C., Drowley, L.,

Plowright, A. T., Needham, E. J., Wang, Q. D., Gregorevic, P., Xin, M., Thomas, W. G., Parton, R. G., Nielsen, L. K., Launikonis, B. S., … Hudson, J. E. (2017). Functional screening in human cardiac organoids reveals a metabolic mechanism for cardiomyocyte cell cycle arrest. *Proceedings of the National Academy of Sciences of the United States of America*, *114*(40), E8372–E8381. https://doi.org/10.1073/pnas.1707316114

Ng, E. S., Sarila, G., Li, J. Y., Edirisinghe, H. S., Saxena, R., Sun, S., Bruveris, F. F., Labonne, T., Sleebs, N., Maytum, A., Yow, R. Y., Inguanti, C., Motazedian, A., Calvanese, V., Capellera-Garcia, S., Ma, F., Nim, H. T., Ramialison, M., Bonifer, C., … Elefanty, A. G. (2024). Long-term engrafting multilineage hematopoietic cells differentiated from human induced pluripotent stem cells. *Nature Biotechnology*. https://doi.org/10.1038/s41587-024-02360-7

Oliveira, M. F., Romero, J. P., Chung, M., Williams, S., Gottscho, A. D., Gupta, A., Pilipauskas, S. E., Mohabbat, S., Raman, N., Sukovich, D., Patterson, D., & Taylor, S. E. B. (2024). *Characterization of immune cell populations in the tumor microenvironment of colorectal cancer using high definition spatial profiling*. https://doi.org/10.1101/2024.06.04.597233

Palla, G., Spitzer, H., Klein, M., Fischer, D., Schaar, A. C., Kuemmerle, L. B., Rybakov, S., Ibarra, I. L., Holmberg, O., Virshup, I., Lotfollahi, M., Richter, S., & Theis, F. J. (2022). Squidpy: a scalable framework for spatial omics analysis. *Nature Methods*, *19*(2), 171–178. https://doi.org/10.1038/s41592-021-01358-2

Pocock, M., Reid, J. D., Robinson, H. R., Charitakis, N., Krycer, J. R., Foster, S. R., Fitzsimmons, R. L., Lor, M., Tuano, N., Howden, S., Vlahos, K., Watt, K. I., Piers, A., Voges, H. K., Fortuna, P. R. J., Rae, J., Parton, R. G., Konstantinov, I. E., Weintraub, R. G., … Hudson, J. E. (2024). *Maturation of human cardiac organoids enables complex disease modelling and drug discovery*. https://doi.org/10.1101/2024.09.05.611336

Prasad, M., Kumar, R., Buragohain, L., Kumari, A., & Ghosh, M. (2021). Organoid Technology: A Reliable Developmental Biology Tool for Organ-Specific Nanotoxicity Evaluation. In *Frontiers in Cell and Developmental Biology* (Vol. 9). Frontiers Media S.A. https://doi.org/10.3389/fcell.2021.696668

StereopyBin. (n.d.). Https://Stereopy.Readthedocs.Io/En/Latest/Tutorials/SquareBin_Clustering.Html.

Uzquiano, A., Kedaigle, A. J., Pigoni, M., Paulsen, B., Adiconis, X., Kim, K., Faits, T., Nagaraja, S., Antón-Bolaños, N., Gerhardinger, C., Tucewicz, A., Murray, E., Jin, X., Buenrostro, J., Chen, F., Velasco, S., Regev, A., Levin, J. Z., & Arlotta, P. (2022). Proper acquisition of cell class identity in organoids allows definition of fate specification programs of the human cerebral cortex. *Cell*, *185*(20), 3770-3788.e27. https://doi.org/10.1016/j.cell.2022.09.010

Vanslambrouck, J. M., Wilson, S. B., Tan, K. S., Soo, J. Y. C., Scurr, M., Spijker, H. S., Starks, L. T., Neilson, A., Cui, X., Jain, S., Little, M. H., & Howden, S. E. (2019). A toolbox to characterize human induced

pluripotent stem cell-derived kidney cell types and organoids. *Journal of the American Society of Nephrology*, *30*(10), 1811–1823. https://doi.org/10.1681/ASN.2019030303

Velasco, S., Kedaigle, A. J., Simmons, S. K., Nash, A., Rocha, M., Quadrato, G., Paulsen, B., Nguyen, L., Adiconis, X., Regev, A., Levin, J. Z., & Arlotta, P. (2019). Individual brain organoids reproducibly form cell diversity of the human cerebral cortex. *Nature*, *570*(7762), 523–527. https://doi.org/10.1038/s41586-019-1289-x

Vlahos, K., Sourris, K., Mayberry, R., McDonald, P., Bruveris, F. F., Schiesser, J. V., Bozaoglu, K., Lockhart, P. J., Stanley, E. G., & Elefanty, A. G. (2019). Generation of iPSC lines from peripheral blood mononuclear cells from 5 healthy adults. *Stem Cell Research*, *34*. https://doi.org/10.1016/j.scr.2018.101380

Voges H. et al. (2025). Bioengineered 3D human heart valve tissues with enhanced maturational properties for disease modelling and therapeutic applications. *Manuscript submitted for publication.*

Voges, H. K., Foster, S. R., Reynolds, L., Parker, B. L., Devilée, L., Quaife-Ryan, G. A., Fortuna, P. R. J., Mathieson, E., Fitzsimmons, R., Lor, M., Batho, C., Reid, J., Pocock, M., Friedman, C. E., Mizikovsky, D., Francois, M., Palpant, N. J., Needham, E. J., Peralta, M., … Hudson, J. E. (2023). Vascular cells improve functionality of human cardiac organoids. *Cell Reports*, *42*(5). https://doi.org/10.1016/j.celrep.2023.112322

Wahle, P., Brancati, G., Harmel, C., He, Z., Gut, G., del Castillo, J. S., Xavier da Silveira dos Santos, A., Yu, Q., Noser, P., Fleck, J. S., Gjeta, B., Pavlinić, D., Picelli, S., Hess, M., Schmidt, G. W., Lummen, T. T. A., Hou, Y., Galliker, P., Goldblum, D., … Camp, J. G. (2023). Multimodal spatiotemporal phenotyping of human retinal organoid development. *Nature Biotechnology*, *41*(12), 1765–1775. https://doi.org/10.1038/s41587-023-01747-2

Waylen, L. N., Nim, H. T., Martelotto, L. G., & Ramialison, M. (2020). From whole-mount to single-cell spatial assessment of gene expression in 3D. In *Communications Biology* (Vol. 3, Issue 1). Nature Research. https://doi.org/10.1038/s42003-020-01341-1

Werder, R. B., Liu, T., Abo, K. M., Lindstrom-Vautrin, J., Villacorta-Martin, C., Huang, J., Hinds, A., Boyer, N., Bullitt, E., Liesa, M., Silverman, E. K., Kotton, D. N., Cho, M. H., Zhou, X., & Wilson, A. A. (2022). CRISPR interference interrogation of COPD GWAS genes reveals the functional significance of desmoplakin in iPSC-derived alveolar epithelial cells. In *Sci. Adv* (Vol. 8).

Williams, C. G., Lee, H. J., Asatsuma, T., Vento-Tormo, R., & Haque, A. (2022). An introduction to spatial transcriptomics for biomedical research. In *Genome Medicine* (Vol. 14, Issue 1). BioMed Central Ltd. https://doi.org/10.1186/s13073-022-01075-1

Yammine, K. M., Mirda Abularach, S., Sampurno, L., Bateman, J. F., Lamandé, S. R., & Shoulders, M. D. (2023). Using CRISPR/Cas9 to generate a heterozygous COL2A1 p.R719C iPSC line (MCRIi019-A-6) model of human precocious osteoarthritis. *Stem Cell Research*, *67*. https://doi.org/10.1016/j.scr.2023.103020

Zhao, D., Lei, W., & Hu, S. (2021). Cardiac organoid — a promising perspective of preclinical model. *Stem Cell Research and Therapy*, *12*(1), 1–10. https://doi.org/10.1186/S13287-021-02340-7/FIGURES/3

Zhao, Z., Chen, X., Dowbaj, A. M., Sljukic, A., Bratlie, K., Lin, L., Fong, E. L. S., Balachander, G. M., Chen, Z., Soragni, A., Huch, M., Zeng, Y. A., Wang, Q., & Yu, H. (2022). Organoids. *Nature Reviews Methods Primers*, *2*(1). https://doi.org/10.1038/s43586-022-00174-y

Abo, K. M., Sainz De Aja, J., Lindstrom-Vautrin, J., Alysandratos, K.-D., Richards, A., Garcia-De-Alba, C., Huang, J., Hix, O. T., Werder, R. B., Bullitt, E., Hinds, A., Falconer, I., Villacorta-Martin, C., Jaenisch, R., Kim, C. F., Kotton, D. N., & Wilson, A. A. (2022). *R E S O U R C E A N D T E C H N I C A L A D V A N C E Air-liquid interface culture promotes maturation and allows environmental exposure of pluripotent stem cell-derived alveolar epithelium*. https://doi.org/10.1172/jci

Chen, A., Liao, S., Cheng, M., Ma, K., Wu, L., Lai, Y., Qiu, X., Yang, J., Xu, J., Hao, S., Wang, X., Lu, H., Chen, X., Liu, X., Huang, X., Li, Z., Hong, Y., Jiang, Y., Peng, J., … Wang, J. (2022). Spatiotemporal transcriptomic atlas of mouse organogenesis using DNA nanoball-patterned arrays. *Cell*, *185*(10), 1777-1792.e21. https://doi.org/10.1016/j.cell.2022.04.003

Chiaradia, I., Imaz-Rosshandler, I., Nilges, B. S., Boulanger, J., Pellegrini, L., Das, R., Kashikar, N. D., & Lancaster, M. A. (2023). Tissue morphology influences the temporal program of human brain organoid development. *Cell Stem Cell*, *30*(10), 1351-1367.e10. https://doi.org/10.1016/j.stem.2023.09.003

Fang, S., Xu, M., Cao, L., Liu, X., Bezulj, M., Tan, L., Yuan, Z., Li, Y., Xia, T., Guo, L., Kovacevic, V., Hui, J., Guo, L., Liu, C., Cheng, M., Lin, L., Wen, Z., Josic, B., Milicevic, N., … Xu, X. (2023). *Stereopy: modeling comparative and spatiotemporal cellular heterogeneity via multi-sample spatial transcriptomics*. https://doi.org/10.1101/2023.12.04.569485

Hawkins, F. J., Suzuki, S., Beermann, M. Lou, Barillà, C., Wang, R., Villacorta-Martin, C., Berical, A., Jean, J. C., Le Suer, J., Matte, T., Simone-Roach, C., Tang, Y., Schlaeger, T. M., Crane, A. M., Matthias, N., Huang, S. X. L., Randell, S. H., Wu, J., Spence, J. R., … Kotton, D. N. (2021). Derivation of Airway Basal Stem Cells from Human Pluripotent Stem Cells. *Cell Stem Cell*, *28*(1), 79-95.e8. https://doi.org/10.1016/j.stem.2020.09.017

Huang, J., Hume, A. J., Abo, K. M., Werder, R. B., Villacorta-Martin, C., Alysandratos, K. D., Beermann, M. Lou, Simone-Roach, C., Lindstrom-Vautrin, J., Olejnik, J., Suder, E. L., Bullitt, E., Hinds, A., Sharma, A., Bosmann, M., Wang, R., Hawkins, F., Burks, E. J., Saeed, M., … Kotton, D. N. (2020). SARS-CoV-2 Infection of Pluripotent Stem Cell-Derived Human Lung Alveolar Type 2 Cells Elicits a Rapid Epithelial-Intrinsic Inflammatory Response. *Cell Stem Cell*, *27*(6), 962-973.e7. https://doi.org/10.1016/j.stem.2020.09.013

Jacob, A., Morley, M., Hawkins, F., McCauley, K. B., Jean, J. C., Heins, H., Na, C. L., Weaver, T. E., Vedaie, M., Hurley, K., Hinds, A., Russo, S. J., Kook, S., Zacharias, W., Ochs, M., Traber, K., Quinton, L. J., Crane, A., Davis, B. R., … Kotton, D. N. (2017). Differentiation of Human Pluripotent Stem Cells into Functional Lung Alveolar Epithelial Cells. *Cell Stem Cell*, *21*(4), 472-488.e10. https://doi.org/10.1016/j.stem.2017.08.014

Lamandé, S. R., Ng, E. S., Cameron, T. L., Kung, L. H. W., Sampurno, L., Rowley, L., Lilianty, J., Patria, Y. N., Stenta, T., Hanssen, E., Bell, K. M., Saxena, R., Stok, K.

S., Stanley, E. G., Elefanty, A. G., & Bateman, J. F. (2023). Modeling human skeletal development using human pluripotent stem cells. *Proceedings of the National Academy of Sciences of the United States of America*, *120*(19). https://doi.org/10.1073/pnas.2211510120

Lawlor, K. T., Vanslambrouck, J. M., Higgins, J. W., Chambon, A., Bishard, K., Arndt, D., Er, P. X., Wilson, S. B., Howden, S. E., Sin Tan, K., Li, F., Hale, L. J., Shepherd, B., Pentoney, S., Presnell, S. C., Chen, A. E., & Little, M. H. (2021). Cellular extrusion bioprinting improves kidney organoid reproducibility and conformation. HHS Public Access. *Nat Mater*, *20*(2), 260–271. https://doi.org/10.6084/m9.figshare.12957122

Lin, Y., Ghazanfar, S., Strbenac, D., Wang, A., Patrick, E., Lin, D. M., Speed, T., Yang, J. Y. H., & Yang, P. (2019). Evaluating stably expressed genes in single cells. *GigaScience*, *8*(9). https://doi.org/10.1093/gigascience/giz106

Ma, S., Wang, W., Zhou, J., Liao, S., Hai, C., Hou, Y., Zhou, Z., Wang, Z., Su, Y., Zhu, Y., Dai, X., Zhao, Y., Liao, S., Cai, Y., & Xu, X. (2024). Lamination-based organoid spatially resolved transcriptomics technique for primary lung and liver organoid characterization. *Proceedings of the National Academy of Sciences of the United States of America*, *121*(46). https://doi.org/10.1073/pnas.2408939121

Mills, R. J., Humphrey, S. J., Fortuna, P. R. J., Lor, M., Foster, S. R., Quaife-Ryan, G. A., Johnston, R. L., Dumenil, T., Bishop, C., Rudraraju, R., Rawle, D. J., Le, T., Zhao, W., Lee, L., Mackenzie-Kludas, C., Mehdiabadi, N. R., Halliday, C., Gilham, D., Fu, L., … Hudson, J. E. (2021). BET inhibition blocks inflammation-induced cardiac dysfunction and SARS-CoV-2 infection. *Cell*, *184*(8), 2167-2182.e22. https://doi.org/10.1016/j.cell.2021.03.026

Mills, R. J., Parker, B. L., Quaife-Ryan, G. A., Voges, H. K., Needham, E. J., Bornot, A., Ding, M., Andersson, H., Polla, M., Elliott, D. A., Drowley, L., Clausen, M., Plowright, A. T., Barrett, I. P., Wang, Q. D., James, D. E., Porrello, E. R., & Hudson, J. E. (2019). Drug Screening in Human PSC-Cardiac Organoids Identifies Pro-proliferative Compounds Acting via the Mevalonate Pathway. *Cell Stem Cell*, *24*(6), 895-907.e6. https://doi.org/10.1016/j.stem.2019.03.009

Mills, R. J., Titmarsh, D. M., Koenig, X., Parker, B. L., Ryall, J. G., Quaife-Ryan, G. A., Voges, H. K., Hodson, M. P., Ferguson, C., Drowley, L., Plowright, A. T., Needham, E. J., Wang, Q. D., Gregorevic, P., Xin, M., Thomas, W. G., Parton, R. G., Nielsen, L. K., Launikonis, B. S., … Hudson, J. E. (2017). Functional screening in human cardiac organoids reveals a metabolic mechanism for cardiomyocyte cell cycle arrest. *Proceedings of the National Academy of Sciences of the United States of America*, *114*(40), E8372–E8381. https://doi.org/10.1073/pnas.1707316114

Ng, E. S., Sarila, G., Li, J. Y., Edirisinghe, H. S., Saxena, R., Sun, S., Bruveris, F. F., Labonne, T., Sleebs, N., Maytum, A., Yow, R. Y., Inguanti, C., Motazedian, A., Calvanese, V., Capellera-Garcia, S., Ma, F., Nim, H. T., Ramialison, M., Bonifer, C., … Elefanty, A. G. (2024). Long-term engrafting multilineage hematopoietic cells differentiated from human induced pluripotent stem cells. *Nature Biotechnology*. https://doi.org/10.1038/s41587-024-02360-7

Oliveira, M. F., Romero, J. P., Chung, M., Williams, S., Gottscho, A. D., Gupta, A., Pilipauskas, S. E., Mohabbat, S., Raman, N., Sukovich, D., Patterson, D., & Taylor, S. E. B. (2024). *Characterization of immune cell populations in the tumor microenvironment of colorectal cancer using high definition spatial profiling*. https://doi.org/10.1101/2024.06.04.597233

Palla, G., Spitzer, H., Klein, M., Fischer, D., Schaar, A. C., Kuemmerle, L. B., Rybakov, S., Ibarra, I. L., Holmberg, O., Virshup, I., Lotfollahi, M., Richter, S., & Theis, F. J.

(2022). Squidpy: a scalable framework for spatial omics analysis. *Nature Methods*, *19*(2), 171–178. https://doi.org/10.1038/s41592-021-01358-2

Pocock, M., Reid, J. D., Robinson, H. R., Charitakis, N., Krycer, J. R., Foster, S. R., Fitzsimmons, R. L., Lor, M., Tuano, N., Howden, S., Vlahos, K., Watt, K. I., Piers, A., Voges, H. K., Fortuna, P. R. J., Rae, J., Parton, R. G., Konstantinov, I. E., Weintraub, R. G., … Hudson, J. E. (2024). *Maturation of human cardiac organoids enables complex disease modelling and drug discovery*. https://doi.org/10.1101/2024.09.05.611336

Prasad, M., Kumar, R., Buragohain, L., Kumari, A., & Ghosh, M. (2021). Organoid Technology: A Reliable Developmental Biology Tool for Organ-Specific Nanotoxicity Evaluation. In *Frontiers in Cell and Developmental Biology* (Vol. 9). Frontiers Media S.A. https://doi.org/10.3389/fcell.2021.696668

StereopyBin. (n.d.). Https://Stereopy.Readthedocs.Io/En/Latest/Tutorials/SquareBin_Clustering.Html.

Uzquiano, A., Kedaigle, A. J., Pigoni, M., Paulsen, B., Adiconis, X., Kim, K., Faits, T., Nagaraja, S., Antón-Bolaños, N., Gerhardinger, C., Tucewicz, A., Murray, E., Jin, X., Buenrostro, J., Chen, F., Velasco, S., Regev, A., Levin, J. Z., & Arlotta, P. (2022). Proper acquisition of cell class identity in organoids allows definition of fate specification programs of the human cerebral cortex. *Cell*, *185*(20), 3770-3788.e27. https://doi.org/10.1016/j.cell.2022.09.010

Vanslambrouck, J. M., Wilson, S. B., Tan, K. S., Soo, J. Y. C., Scurr, M., Spijker, H. S., Starks, L. T., Neilson, A., Cui, X., Jain, S., Little, M. H., & Howden, S. E. (2019). A toolbox to characterize human induced pluripotent stem cell-derived kidney cell types and organoids. *Journal of the American Society of Nephrology*, *30*(10), 1811–1823. https://doi.org/10.1681/ASN.2019030303

Velasco, S., Kedaigle, A. J., Simmons, S. K., Nash, A., Rocha, M., Quadrato, G., Paulsen, B., Nguyen, L., Adiconis, X., Regev, A., Levin, J. Z., & Arlotta, P. (2019). Individual brain organoids reproducibly form cell diversity of the human cerebral cortex. *Nature*, *570*(7762), 523–527. https://doi.org/10.1038/s41586-019-1289-x

Vlahos, K., Sourris, K., Mayberry, R., McDonald, P., Bruveris, F. F., Schiesser, J. V., Bozaoglu, K., Lockhart, P. J., Stanley, E. G., & Elefanty, A. G. (2019). Generation of iPSC lines from peripheral blood mononuclear cells from 5 healthy adults. *Stem Cell Research*, *34*. https://doi.org/10.1016/j.scr.2018.101380

Voges H. et al. (2025). *Bioengineered 3D human heart valve tissues with enhanced maturational properties for disease modelling and therapeutic applications*.

Voges, H. K., Foster, S. R., Reynolds, L., Parker, B. L., Devilée, L., Quaife-Ryan, G. A., Fortuna, P. R. J., Mathieson, E., Fitzsimmons, R., Lor, M., Batho, C., Reid, J., Pocock, M., Friedman, C. E., Mizikovsky, D., Francois, M., Palpant, N. J., Needham, E. J., Peralta, M., … Hudson, J. E. (2023). Vascular cells improve functionality of human cardiac organoids. *Cell Reports*, *42*(5). https://doi.org/10.1016/j.celrep.2023.112322

Wahle, P., Brancati, G., Harmel, C., He, Z., Gut, G., del Castillo, J. S., Xavier da Silveira dos Santos, A., Yu, Q., Noser, P., Fleck, J. S., Gjeta, B., Pavlinić, D., Picelli, S., Hess, M., Schmidt, G. W., Lummen, T. T. A., Hou, Y., Galliker, P., Goldblum, D., … Camp, J. G. (2023). Multimodal spatiotemporal phenotyping of human retinal organoid development. *Nature Biotechnology*, *41*(12), 1765–1775. https://doi.org/10.1038/s41587-023-01747-2

Waylen, L. N., Nim, H. T., Martelotto, L. G., & Ramialison, M. (2020). From whole-mount to single-cell spatial assessment of gene expression in 3D. In

Communications Biology (Vol. 3, Issue 1). Nature Research. https://doi.org/10.1038/s42003-020-01341-1

Werder, R. B., Liu, T., Abo, K. M., Lindstrom-Vautrin, J., Villacorta-Martin, C., Huang, J., Hinds, A., Boyer, N., Bullitt, E., Liesa, M., Silverman, E. K., Kotton, D. N., Cho, M. H., Zhou, X., & Wilson, A. A. (2022). CRISPR interference interrogation of COPD GWAS genes reveals the functional significance of desmoplakin in iPSC-derived alveolar epithelial cells. In *Sci. Adv* (Vol. 8).

Williams, C. G., Lee, H. J., Asatsuma, T., Vento-Tormo, R., & Haque, A. (2022). An introduction to spatial transcriptomics for biomedical research. In *Genome Medicine* (Vol. 14, Issue 1). BioMed Central Ltd. https://doi.org/10.1186/s13073-022-01075-1

Yammine, K. M., Mirda Abularach, S., Sampurno, L., Bateman, J. F., Lamandé, S. R., & Shoulders, M. D. (2023). Using CRISPR/Cas9 to generate a heterozygous COL2A1 p.R719C iPSC line (MCRIi019-A-6) model of human precocious osteoarthritis. *Stem Cell Research*, *67*. https://doi.org/10.1016/j.scr.2023.103020

Zhao, D., Lei, W., & Hu, S. (2021). Cardiac organoid — a promising perspective of preclinical model. *Stem Cell Research and Therapy*, *12*(1), 1–10. https://doi.org/10.1186/S13287-021-02340-7/FIGURES/3

Zhao, Z., Chen, X., Dowbaj, A. M., Sljukic, A., Bratlie, K., Lin, L., Fong, E. L. S., Balachander, G. M., Chen, Z., Soragni, A., Huch, M., Zeng, Y. A., Wang, Q., & Yu, H. (2022). Organoids. *Nature Reviews Methods Primers*, *2*(1). https://doi.org/10.1038/s43586-022-00174-y

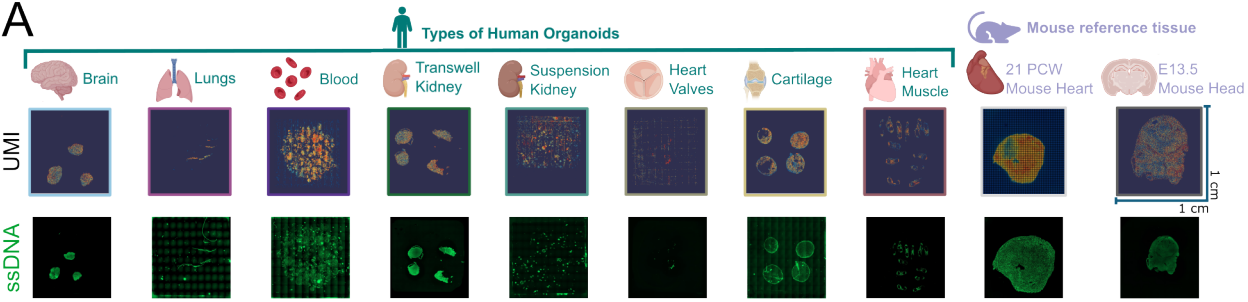

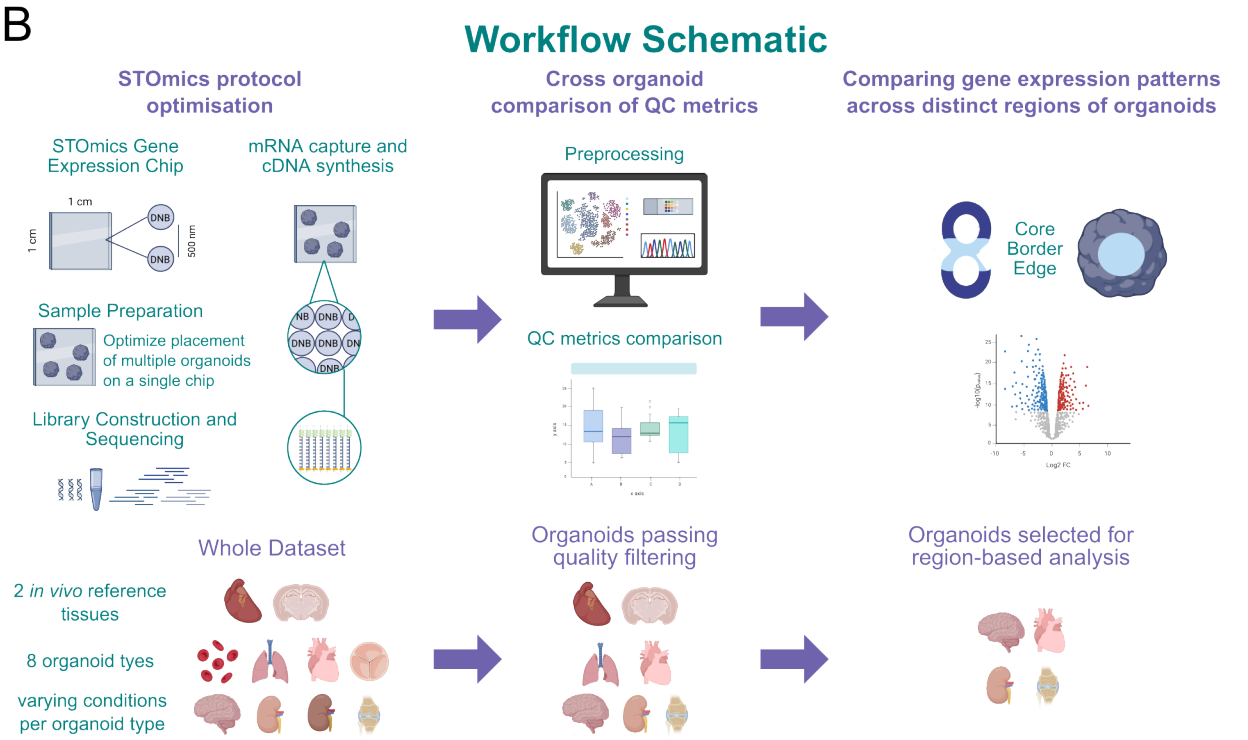

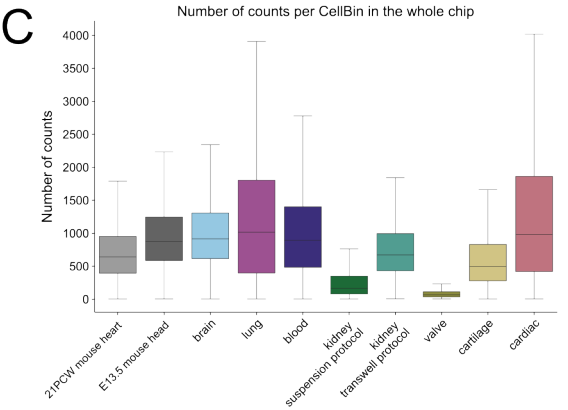

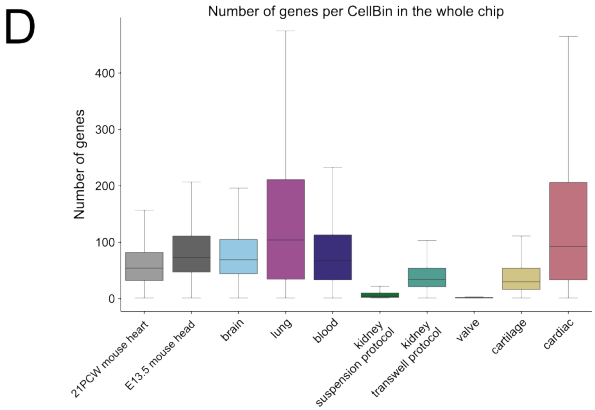

Nucera, Charitakis, Leung et al Fig1

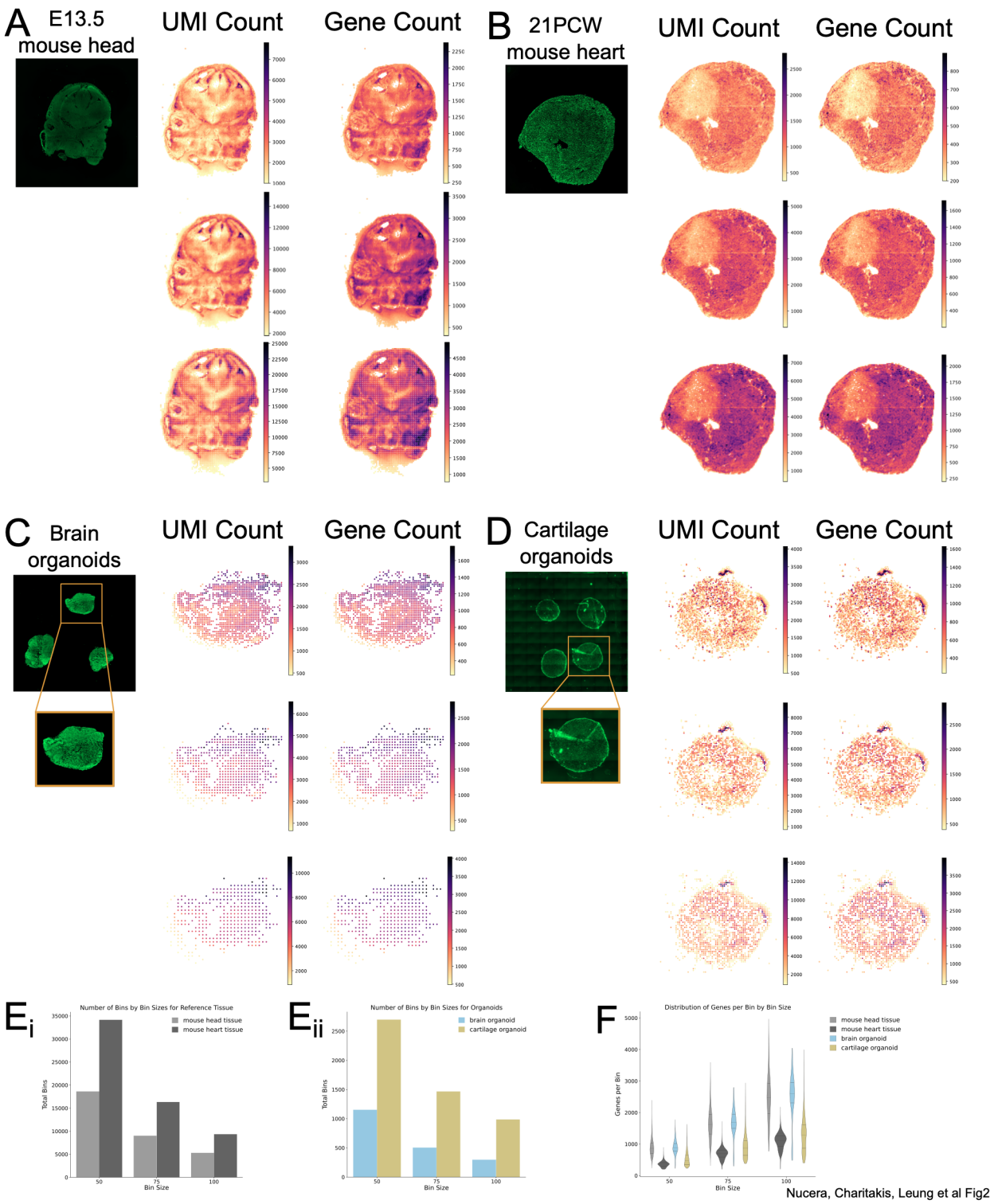

Nucera, Charitakis, Leung et al Fig2

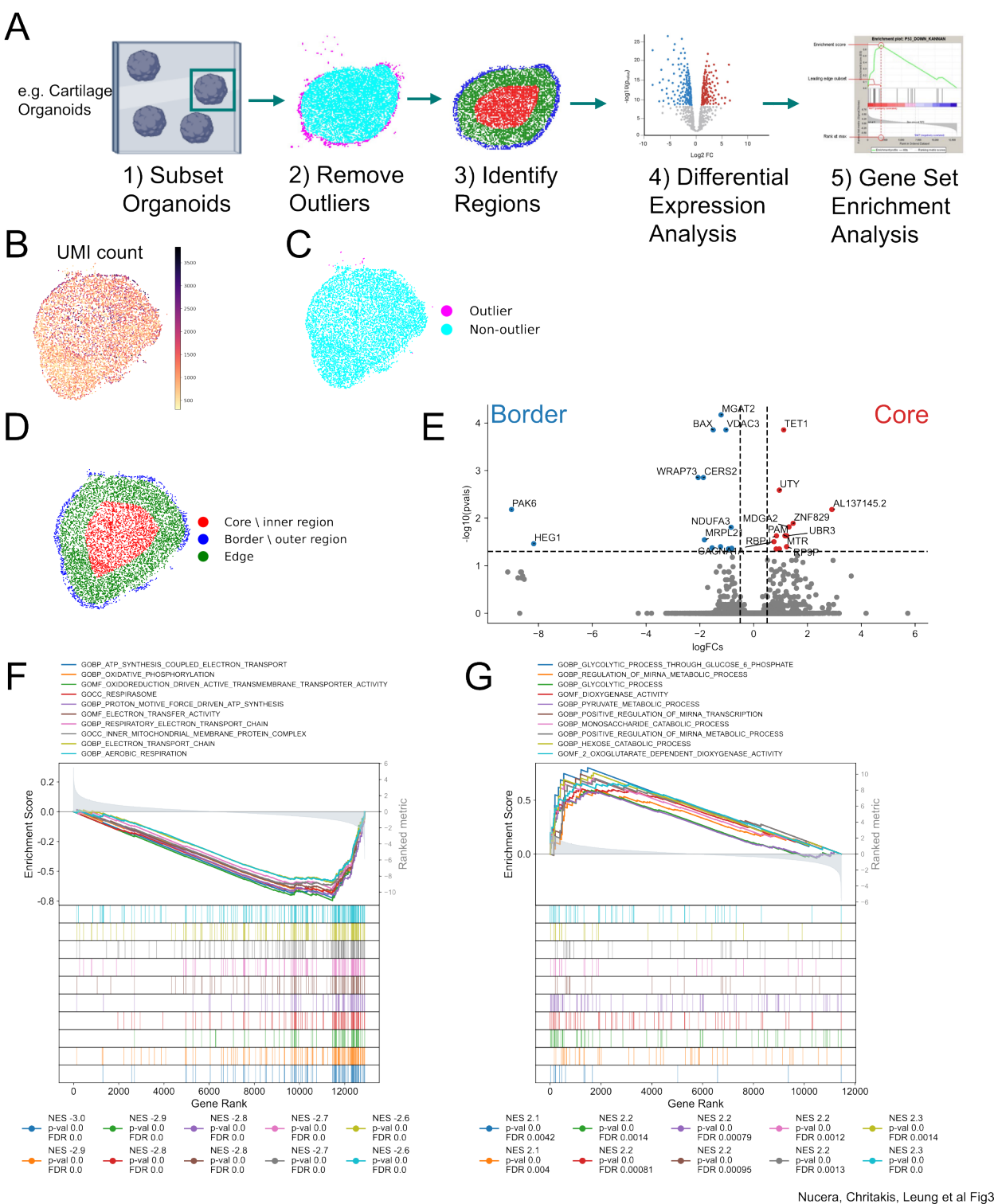

Nucera, Chritakis, Leung et al Fig3

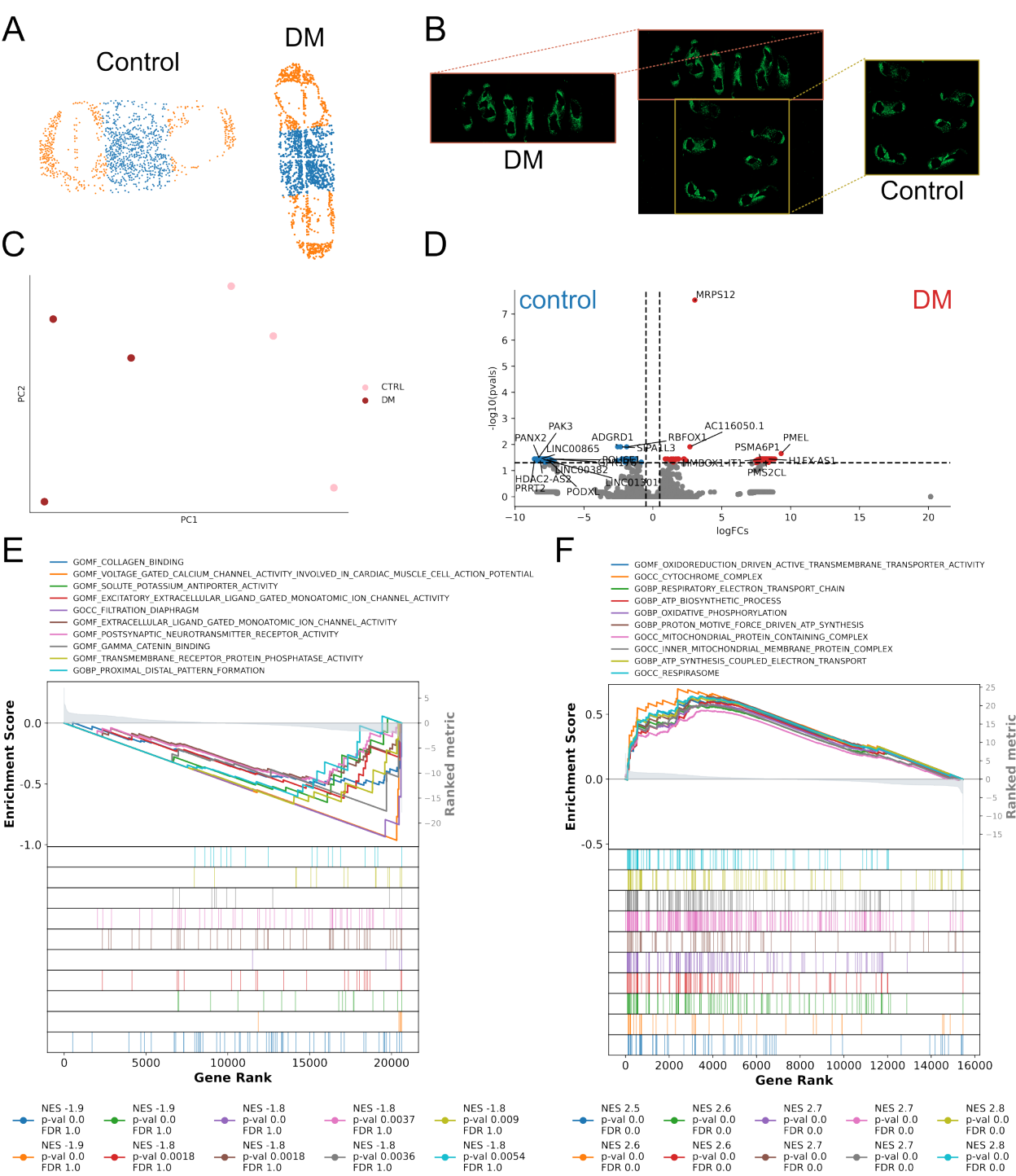

Nucera, Charitakis, Leung et al Fig4